Supporting Information

Co-doped MnO_2 with abundant oxygen vacancies as cathode for superior aqueous magnesium ion storage

Liming Xu,[a#] Guodong Pan,[a#] Caiyan Yu,[b*] Jiabao Li,[c] Zhiwei Gong,[d] Ting Lu,[a*] Likun Pan[a*]

[a] *Shanghai Key Laboratory of Magnetic Resonance, School of Physics and Electronic Science, East China Normal University, Shanghai 200241, China*

[b] *International Joint Laboratory of Renewable Energy Materials and Devices of Henan Province and School of Physics & Electronics, Henan University, Kaifeng 475004, P.R. China*

[c] *School of Chemistry and Chemical Engineering, Yanghou University, Yangzhou, Jiangsu 225002, China*

[d] *School of Physics and Electronic Science, East China Normal University, Shanghai 200241, China*

**Corresponding authors*

Email: lkpan@phy.ecnu.edu.cn (Likun Pan); cyyu@henu.edu.cn (Caiyan Yu); tlu@phy.ecnu.edu.cn (Ting Lu)

[#] *Author Contributions: Liming Xu and Guodong Pan contributed equally*

Preparation of working electrode

80 wt% active material, 10 wt% Super P (conductive agent), and 10 wt% polyvinylidene fluoride (binder) were mixed together in 1-methyl-2-pyrrolidone to form a homogeneous slurry. Then, the slurry was uniformly casted on graphite substrates (4 cm^2). Finally, the working electrode was dried in a blast drying oven at 60 °C for 48 h. The loading mass of active substance on working electrode is about 4 mg cm^{-2}.

Electrochemical calculation

For the three-electrode, the specific capacitance (C_{g1}, F g^{-1}) was calculated from the GCD curves according to the following equation[1,2]:

$$C_{g1} = \frac{I \times \Delta t}{m \times \Delta V}$$

where I, ΔV, m and v refer to the current (A), potential window (V), mass of active material (g), and scan rate (V s^{-1}), respectively.

For the two-electrode system, the specific capacitance (C_{g2}, F g^{-1}), the energy density (E, Wh Kg^{-1}), and energy density (P, W Kg^{-1}) were calculated f according to the following equation[3-5]:

$$C_{g2} = \frac{I \times \Delta t}{m \times \Delta V}$$

$$E = \frac{C_g \times \Delta V^2}{2 \times 3.6}$$

$$P = \frac{3600 \times E}{\Delta t}$$

where I, m, ΔV, and Δt refer to the current (A), mass of active material (g), potential window (V), and scan rate (s), respectively.

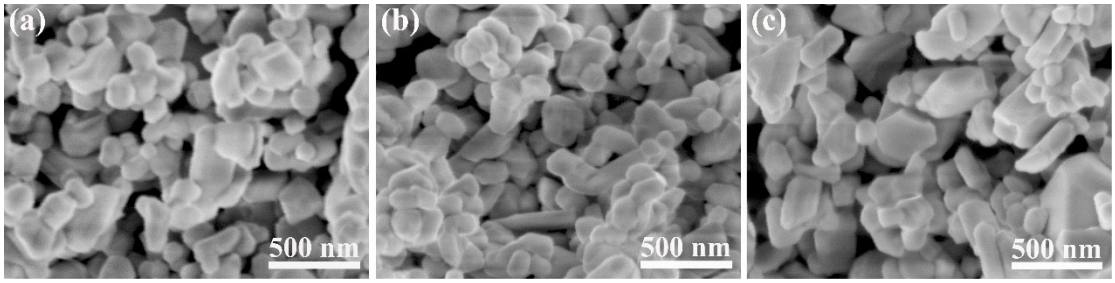

Fig. S1. SEM images of (a) Co-MnO_2-1, (b) Co-MnO_2-3, and (c) Co-MnO_2-4.

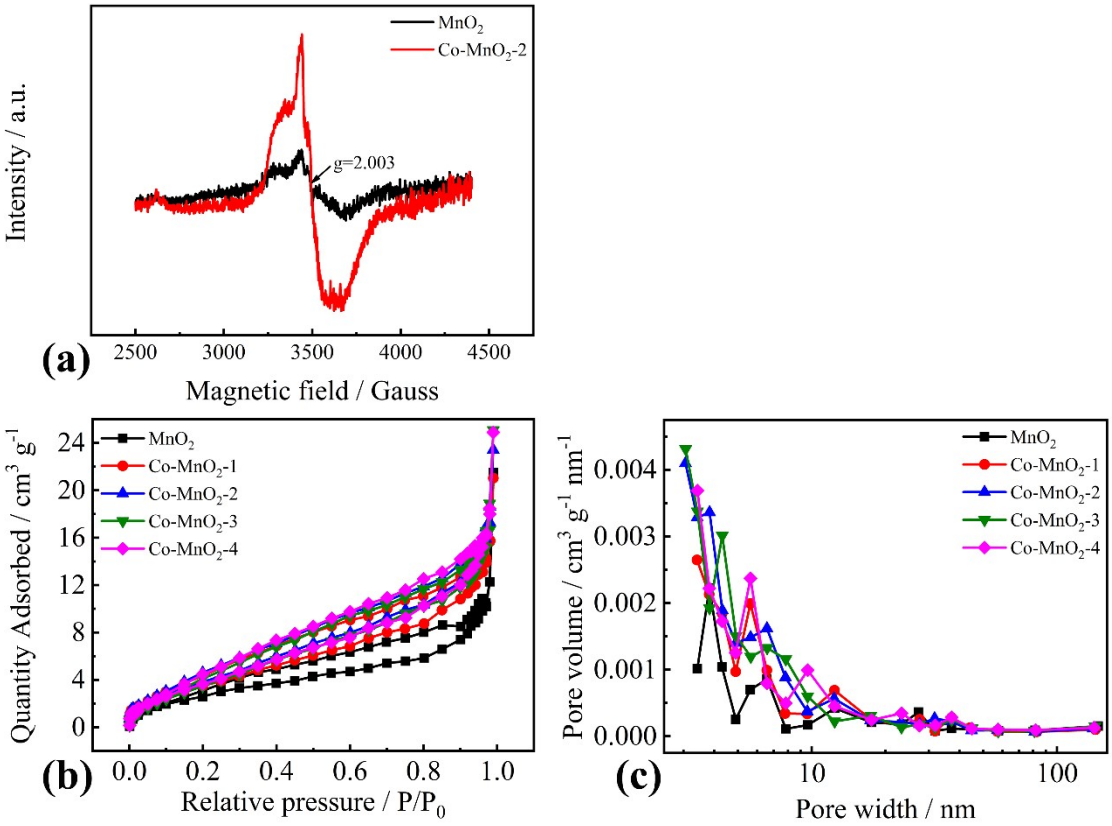

Fig. S2. (a) EPR spectra for the MnO_2 and Co-MnO_2-2. (b) BET adsorption-desorption isotherms and (c) pore size distributions of MnO_2, Co-MnO_2-1, Co-MnO_2-2, Co-MnO_2-3, and Co-MnO_2-4.

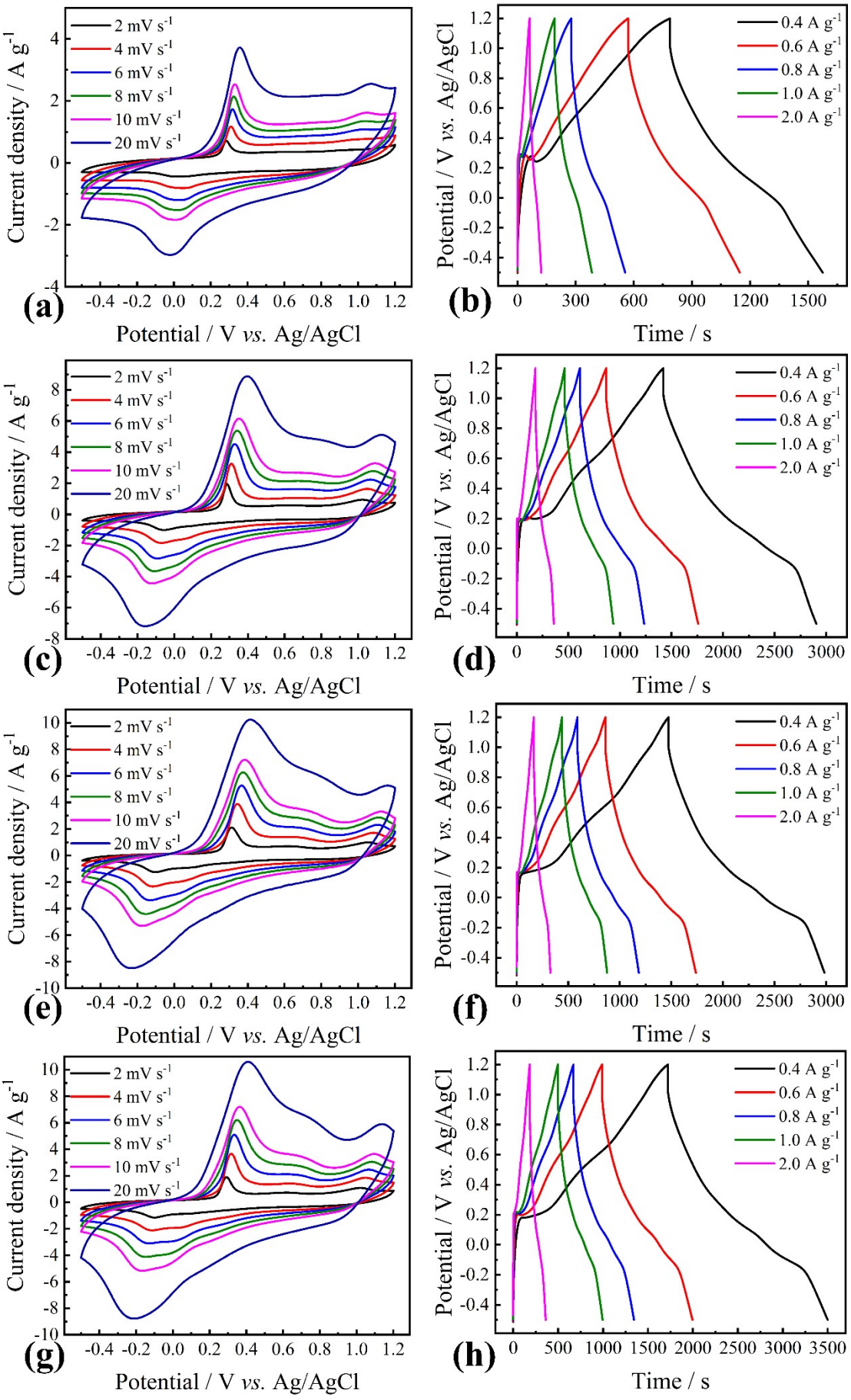
(a)
Current density / A g-1
Potential / V vs. Ag/AgCl
2 mV s-1
4 mV s-1
6 mV s-1
8 mV s-1
10 mV s-1
20 mV s-1
(b)
Potential / V vs. Ag/AgCl
Time / s
0.4 A g-1
0.6 A g-1
0.8 A g-1
1.0 A g-1
2.0 A g-1
(c)
(d)
(e)
(f)
(g)
(h)

Fig. S3. CV curves at varied scan rates and GCD curves at 0.4-2.0 A g^{-1} of (a, b) MnO_2, (c, d) Co-MnO_2-1, (e, f) Co-MnO_2-3, and (g, h) Co-MnO_2-4.

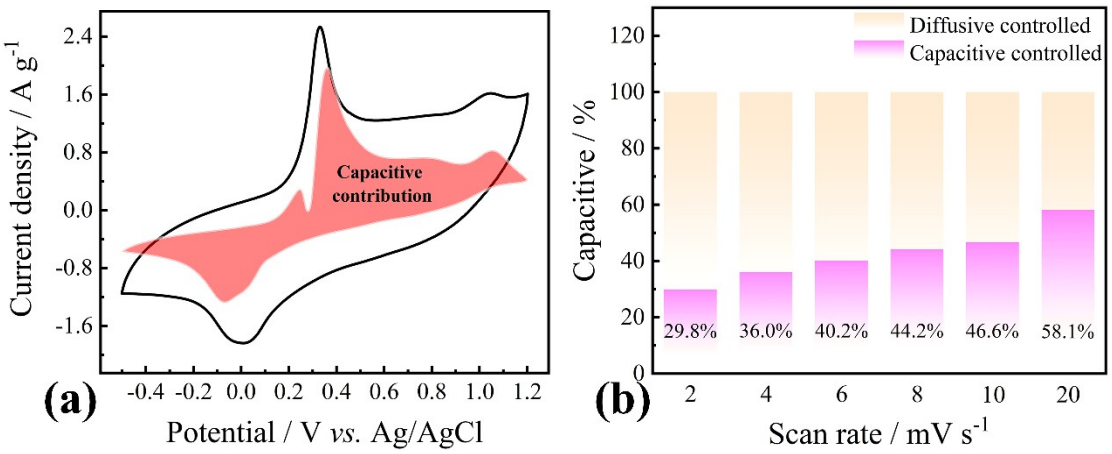

Fig. S4. (a) CV curve with the capacitive contribution at a scan rate of 10 mV s^{-1}, (b) the percentages of capacitive and diffusion contributions of MnO_2.

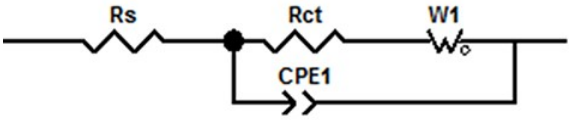

Fig. S5. Equivalent circuit diagram for the Nyquist plots of MnO_2, Co-MnO_2-1, Co-MnO_2-2, Co-MnO_2-3, and Co-MnO_2-4.

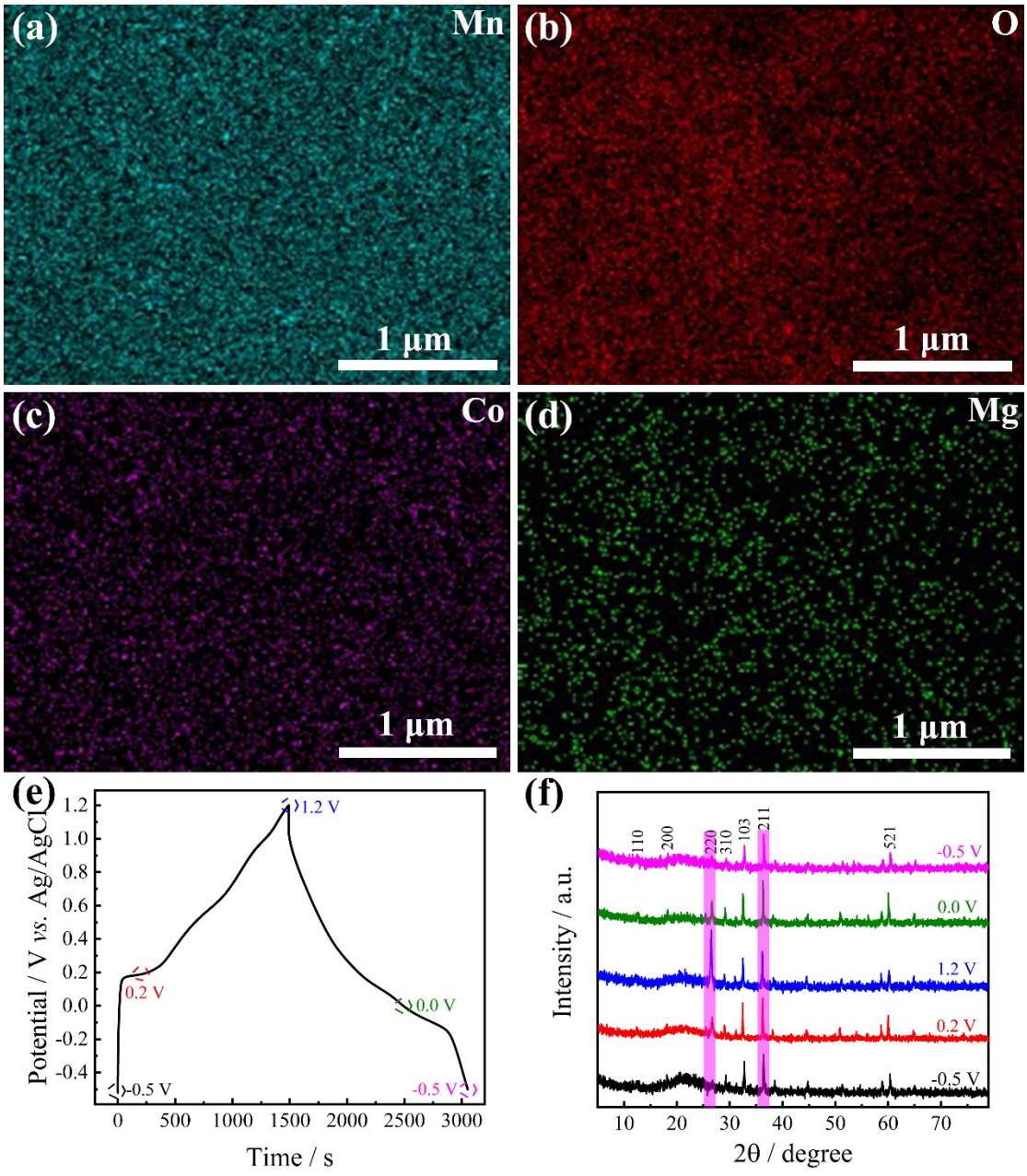

Fig. S6. Elemental mapping images of (a) Mn, (b) O, (c) Co, and (d) Mg of Co-MnO_2-2 electrode charged to 1.2 V. (e) GCD curve of Co-MnO_2-2 at 0.5 A g^{-1}, (f) XRD pattern of Co-MnO_2-2 electrode during the charge/discharge process.

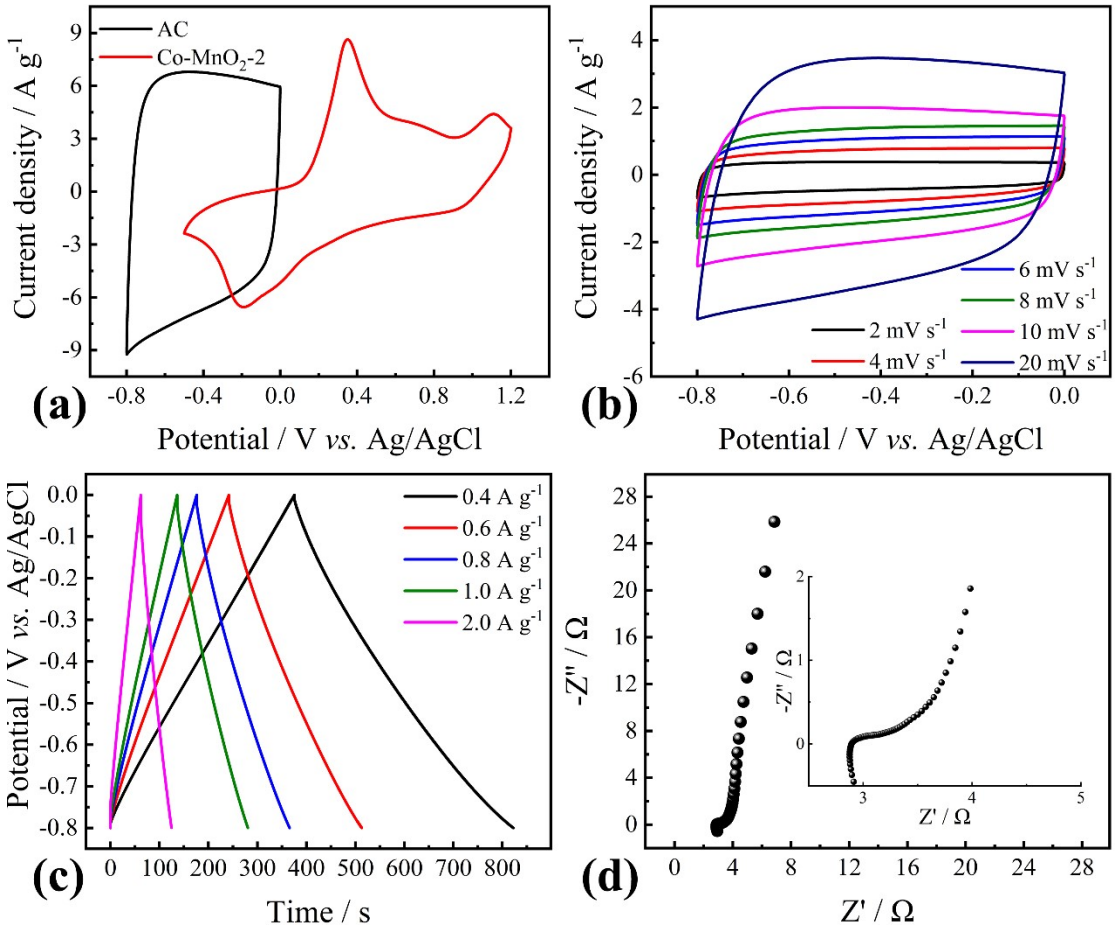

Fig. S7. (a) CV curves of AC and Co-MnO_2-2 at a scan rate of 10 mV s^{-1}. (b) CV curves at 2-20 mV s^{-1}, (c) GCD curve at 0.5-2.0 A g^{-1}, and (d) Nyquist plot of AC.

Table S1. The contents of Co in Co-MnO_2.

Material	Content of Co
Co-MnO_2-1	3.84%
Co-MnO_2-2	7.66%
Co-MnO_2-3	10.74%
Co-MnO_2-4	12.04%

Table S2. The Conductivities of MnO_2, Co-MnO_2-1, Co-MnO_2-2, Co-MnO_2-3, and Co-MnO_2-4.

Material	Conductivity/μS cm^{-1}
MnO_2	3.69
Co-MnO_2-1	50.95
Co-MnO_2-2	346.21
Co-MnO_2-3	17.95
Co-MnO_2-4	6.45

References

S1 L.M. Xu, D.H. Zhu, W.Q. Zhou, F.X. Jiang, Y.L. Wu, Y. Cai, H. Kang and J.K. Xu, One-step hydrothermal synthesis of N-doped graphene/poly5-hydroxyindole composite materials for supercapacitor with ultra-long cycle stability and ultra-high energy storage performance, *J. Energy Storage*, 2021, **43**, 103303.

S2 L.H. Wang, X.K. Ye, Y.C. Zhu, H.D. Jiang, J.X. Xia, Z.Y. Yue, Z.Q. Wan, C.Y. Jia and X.J. Yao, Conjugated molecule functionalized graphene films for energy storage devices with high energy density, *Electrochim. Acta*, 2020, **340**, 135804.

S3 L.M. Xu, Y.Y. Zhang, W.Q. Zhou, F.X. Jiang, H. Zhang, Q.L. Jiang, Y.H. Jia, R. Wang, A.Q. Liang, J.K. Xu and X.M. Duan, Fused Heterocyclic Molecule-Functionalized N-Doped Reduced Graphene Oxide by Non-Covalent Bonds for High-Performance Supercapacitors, *ACS Appl. Mater. Interfaces 2020*, **12**, 45202-45213.

S4 J.W. Zhang, L.B. Zhu, H.T. Jia, K.X. Wei and L.X. Wen, Microreactor facilitated

preparation and Ni-doping of MnO2 nanoparticles for supercapacitors, *J. Alloys Compd.*, 2021, **889**, 161772.

S5 N. Zarshad, A.U. Rahman, J.H. Wu, A. Ali, F. Raziq, L. Han, P. Wang, G.G. Li and H.M. Ni, Enhanced energy density and wide potential window for K incorporated MnO_2@carbon cloth supercapacitor, *Chem. Eng. J.*, 2021, **415**, 128967.